ACS APPLIED MATERIALS & INTERFACES

Research Article

Cite This: ACS Appl. Mater. Interfaces 2019, 11, 10707−10717

www.acsami.org

Highly Electrocatalytic, Durable, and Stretchable Nanohybrid Fiber for On-Body Sweat Glucose Detection

Phan Tan Toi,[†] Tran Quang Trung,[†] Thi My Linh Dang,[†] Chan Wool Bae,[†] and Nae-Eung Lee*[,†,‡,§]

[†]School of Advanced Materials Science & Engineering, [‡]SKKU Advanced Institute of Nanotechnology, and [§]Samsung Advanced Institute for Health Sciences & Technology, Sungkyunkwan University, Suwon, Kyunggi-do 16419, Korea

Supporting Information

ABSTRACT: A conformal patch biosensor that can detect biomolecules is one promising technology for wearable sweat glucose self-monitoring. However, developing such a patch is challenging because conferring stretchability to its components is difficult. Herein, we demonstrate a platform for a nonenzymatic, electrochemical sensor patch: a wrinkled, stretchable, nanohybrid fiber (WSNF) in which Au nanowrinkles partially cover the reduced graphene oxide (rGO)/polyurethane composite fiber. The WSNF has high electrocatalytic activity because of synergetic effects between the Au nanowrinkles and the oxygen-containing functional groups on the rGO-supporting matrix which promote the dehydrogenation step in glucose oxidation. The WSNF offers stretchability, high sensitivity, low detection limit, high selectivity against interferents, and high ambient-condition stability, and it can detect glucose in neutral conditions. If this WSNF sensor patch were sewn onto a stretchable fabric and attached to the human body, it could continuously measure glucose levels in sweat to accurately reflect blood glucose levels.

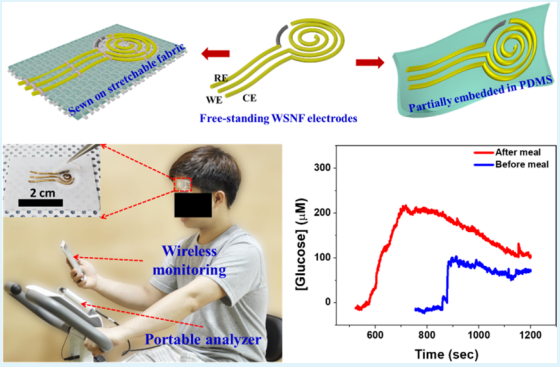

KEYWORDS: *stretchable electrochemical sensor, wearable sweat glucose sensor, nanohybrid fiber, non-enzymatic sensor, on-body monitoring*

INTRODUCTION

Personal monitoring of glucose concentration by using an electrochemical glucose meter and finger-pricked blood plays an important role in managing diabetes.[1] However, existing portable devices require inconvenient, invasive sampling and cannot provide continuous monitoring. For convenient, painless, and automated continuous glucose monitoring, new glucose self-monitoring systems have been proposed, including contact lenses,[2,3] watches,[4] tattoos,[5] and patches,[6−11] which collect their information from tears,[2,3] interstitial fluid,[4,5,8] or sweat.[6,7,9,10] Among these technologies, patch-type wearable glucose sensor systems can be mounted to the human body to continuously and noninvasively determine the glucose levels in sweat.[6,7,9−11]

Recently, a few wearable patches containing enzymatic electrochemical biosensors have been developed and interfaced with a flexible signal processing unit[10,11] or portable electrochemical analyzer[6,9] to measure glucose levels in sweat and transmit the results to a mobile device. Those approaches could assist wearers in the personal diagnosis and monitoring of health conditions in their homes, schools, workplaces, and sports facilities. Even though most previous works have investigated enzymatic electrochemical sensors with mechanical flexibility, conformal attachment of the sensors to the human skin during daily activities remains limited.[11] Thus, a wearable patch containing a stretchable, enzymatic, electrochemical biosensor would be advantageous, providing a conformal contact with the skin and adjusting itself to the skin deformations induced by the wearer's activities.[6,7,9] However, stretchable enzymatic electrochemical glucose biosensors can be degraded by long-term storage,[12,13] temperature,[14] or pH,[14] which can cause instability in their sensing performance.

As an alternative to a stretchable, enzymatic, electrochemical sensor, a stretchable, nonenzymatic electrochemical sensor that uses electrocatalytic materials such as metal oxides,[15−18] alloys,[19,20] metal nanomaterials,[21−24] and carbon nanocomposites[25−28] to directly oxidize glucose might be an attractive approach. Extensive research on nonenzymatic electrochemical biosensors for the detection of glucose has been done using a rigid substrate.[16−18,21−26] One stretchable nonenzymatic glucose sensor was proposed for glucose detection in sweat,[29] but the sensing device required multiple steps for fabrication and was not capable of continuous on-body glucose monitoring. In developing a stretchable, nonenzymatic glucose sensor, imparting mechanical stretchability to the electrocatalytic materials is the most important and daunting task. A simple fabrication process for a stretchable, nonenzymatic

Received: November 22, 2018
Accepted: February 27, 2019
Published: February 27, 2019

DOI: 10.1021/acsami.8b20583
ACS Appl. Mater. Interfaces 2019, 11, 10707−10717

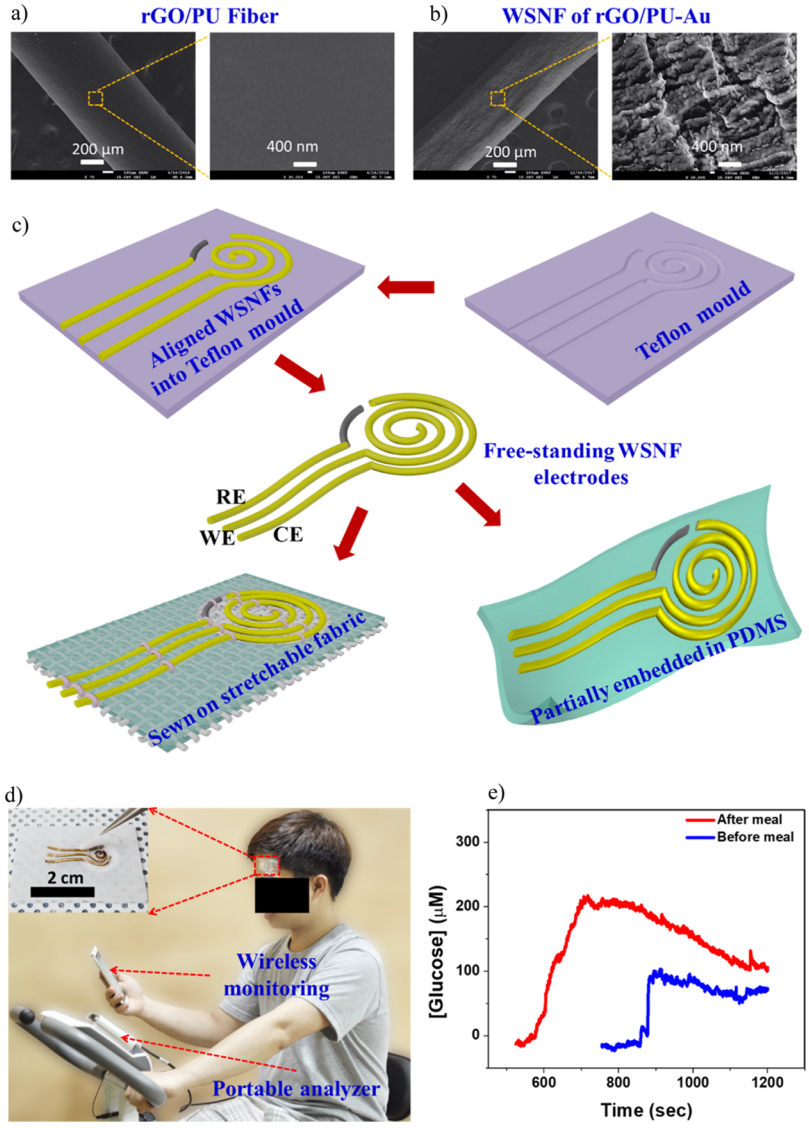

Figure 1. Architecture and fundamental characteristics of the WSNF used as an electrochemical sweat glucose sensor. (a) Field-emission scanning electron microscopy (FE-SEM) images of the rGO/PU nanocomposite fiber. (b) FE-SEM images of WSNF of rGO/PU/Au. (c) Schematic diagram of the fabrication process for free-standing WSNF electrodes (CE, WE, and RE) partially embedded on a PDMS substrate or sewn onto stretchable fabric to produce a stretchable WSNF glucose sensor. (d) WSNF glucose sensor sewn onto a stretchable fabric (inset) and attached to the forehead of a human body. (e) Continuous on-body monitoring of glucose levels in sweat before and after meals.

glucose sensor that could be integrated into a wearable form would open new possibilities for wearable devices for glucose self-monitoring.

Herein, we propose highly electrocatalytic, wrinkled, stretchable nanohybrid fibers (WSNFs) made of reduced graphene oxide–polyurethane (rGO/PU) with gold (Au) nanowrinkles for use as a nonenzymatic electrochemical biosensor that can perform continuous glucose monitoring in sweat. A new design of free-standing WSNFs with a high total surface area of Au nanowrinkles that partially covers the rGO/PU composite fiber can provide high electrocatalytic effect, stretchability, and durability under mechanical deformation. Synergetic effects between the Au nanowrinkles and the rGO supporting matrix, which contains oxygen-containing functional groups, are presumed to enhance the sensor's electrocatalytic activity by inducing abundant hydroxide anions onto the surface of Au nanowrinkles ($Au(OH)_{abs}$) to promote dehydrogenation in the glucose oxidation reaction. Therefore, the WSNF electrode exhibits high responsivity to glucose, with high sensitivity (140 $\mu A \cdot mM^{-1} \cdot cm^{-2}$), low detection limit (500 nM), high selectivity against interferents, and stability under ambient conditions, and it can detect glucose in neutral solution conditions. The stretchable glucose sensor is composed of WSNFs as the working electrode (WE), a counter electrode (CE), and a reference electrode (RE) modified with Ag/Ag/Cl. It has stretchability up to 30% and stable responses after 10 000 stretching cycles at 30% strain. Furthermore, the sensor patch can be fabricated by directly sewing the WSNF electrodes onto a stretchable fabric. We demonstrated its function by attaching it to the human body and continuously measuring glucose levels in sweat through a portable electrochemical analyzer wirelessly connected to a smartphone. The results indicate that the glucose concentration in sweat is closely correlated with that in blood both before and after ingestion.[6,9,29,30] This stretchable nonenzymatic glucose sensor based on WSNFs, which have a

DOI: 10.1021/acsami.8b20583
ACS Appl. Mater. Interfaces 2019, 11, 10707−10717

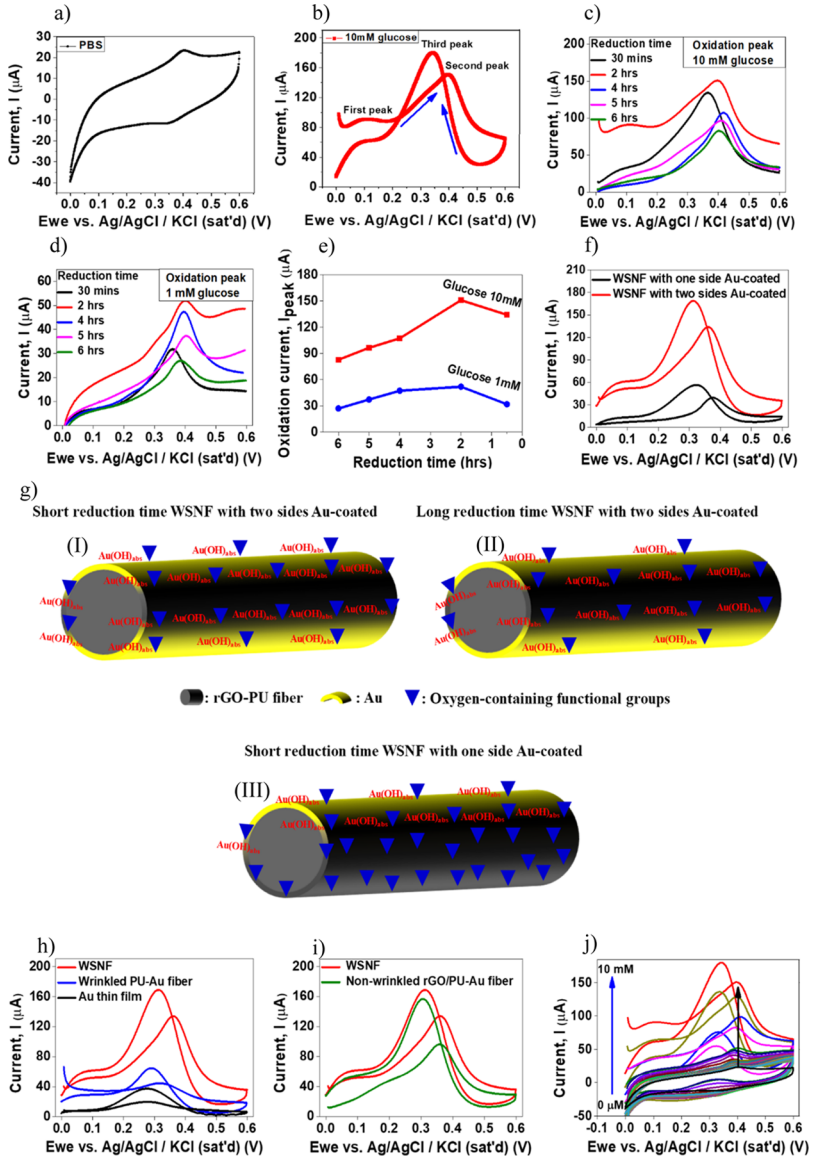

Figure 2. Electrochemical response of the WSNF electrode to glucose. (a) CV curves of the WSNF electrode in PBS. (b) CV curves of the WSNF electrode in PBS with 10 mM glucose. (c) CV curves (second oxidation peak) of WSNF electrodes fabricated with various reduction times in PBS with 10 mM glucose. (d) CV curves (second oxidation peak) of WSNF electrodes fabricated with various reduction times in PBS with 1 mM glucose. (e) I_{peak} data from WSNF electrodes as a function of reduction time. (f) CV curves of WSNF electrodes with one side or two sides coated in Au in PBS with 10 mM glucose concentration. (g) Schematic diagram of the formation of the $Au(OH)_{abs}$ layer on WSNF electrodes fabricated using various conditions: (I) short-reduction-time WSNF coated with Au on two sides, (II) long-reduction-time WSNF coated with Au on two sides, and (III) short-reduction-time WSNF coated with Au on one side. (h) CV curves of WSNF, wrinkled PU/Au fiber, and Au thin film electrodes in PBS with 10 mM glucose. (i) CV curves of WSNF and nonwrinkled rGO/PU/Au nanohybrid fiber electrodes in PBS with 10 mM glucose. (j) CV curves of the WSNF electrode in PBS with various glucose concentrations.

simple fabrication route, is promising because of its direct and facile integrability into fabric or clothes for continuous on-body measurement of glucose levels in sweat.

RESULTS AND DISCUSSION

Free-standing WSNFs, with a large surface of highly wrinkled Au on a functional supporting matrix of the rGO/PU composite fiber, were generated using a stretch-release method. First, a free-standing elastomeric rGO/PU nanocomposite fiber containing 3.5 wt % of rGO, which has an average diameter of 500 μm and a smooth surface (Figure 1a), was fabricated via a wet spinning method (Figure S1). Then, a 5 nm-thick Cr layer (for adhesion promotion) and a 60 nm-thick Au layer were deposited in sequence by e-beam and thermal evaporation, respectively, on the two sides of the nanocomposite fiber under 100% prestretched conditions, and the Au-coated nanocomposite fiber was released to generate a free-standing WSNF rGO/PU/Au hybrid (Figure S2). Two salient features of this WSNF are the formation of Au nanowrinkles on the surface and the partial coverage of the Au layer on the rGO/PU nanocomposite fiber (Figure 1b). To confirm the mechanical stretchability and durability, we studied the electrical properties of the WSNFs under applied mechanical deformation. The results show that the WSNF can be stretched up to 50% with a very small change in the electrical current (Figure S3). To apply the fabricated WSNFs

DOI: 10.1021/acsami.8b20583
ACS Appl. Mater. Interfaces 2019, 11, 10707−10717

to a stretchable electrochemical sensor, we fabricated three-electrode electrochemical devices using the WSNFs as the WE, CE, and RE. The WSNF electrodes were partially embedded into a polydimethylsiloxane (PDMS) substrate or sewn onto the stretchable fabric to create stretchable electrochemical glucose sensors (Figure 1c). The WSNF glucose sensor integrated with fabric was simply interfaced with a portable electrochemical analyzer and attached to the forehead of a human body (Figure 1d) for continuous on-body monitoring of glucose levels in sweat before and after meals (Figure 1e).

To investigate the fundamental electrochemical glucose oxidation characteristics of the fabricated WSNFs with two Au-coated sides, we affixed the WSNFs to a glass substrate as a WE and used a commercial Ag/AgCl/saturated KCl and Pt wire as the RE and CE, respectively (Figure S4). To ensure that the WSNFs would function as a wearable electrochemical nonenzymatic glucose biosensor for continuous on-body monitoring, we evaluated their performance at the physiological pH of the body fluid (neutral condition). Normally, nonenzymatic electrochemical biosensors require an alkaline condition for the electrocatalytic oxidation of glucose,[15] which can limit their usability as wearable on-body monitors of glucose levels in sweat. Therefore, we first investigated the catalytic performance of the glucose oxidation reaction of the WSNFs in neutral phosphate buffered saline (PBS). The appearance of a broad peak at ~0.4 V in the cyclic voltammogram (CV) curves in a 0.1 M PBS (pH 7.4) implies the chemisorption of hydroxide anions onto the surface of the Au nanowrinkles ($Au(OH)_{abs}$) (Figure 2a). This phenomenon was demonstrated in previous reports that used Au nanostructures as a WE.[31−35] To demonstrate the ability of the WSNFs (as a WE) to detect glucose under neutral conditions, we measured the CV curves in 0.1 M PBS containing 10 mM glucose at a scan rate of 50 mV/s. In the positive potential scan, the results showed the occurrence of two anodic oxidation peaks (Figure 2b). The first peak at the potential of ~0.1 V is due to the formation of $Au(OH)_{abs}$ and adsorption of glucose to form intermediates. Also, the second peak at the potential of ~0.4 V arises from oxidation of the intermediates to gluconolactone under the catalytic effect of Au(OH). During the negative scan, the third peak at ~0.3 V (Figure 2b) refers to the reduction of gold oxide to form a fresh gold surface. These results indicate that the formation of $Au(OH)_{abs}$ on the surface of the Au nanowrinkles is approximately correlated with the onset of the electro-oxidation of glucose. Therefore, we suggest that the $Au(OH)_{abs}$ is a catalytic component on the Au surface and plays an important role in glucose oxidation.[34,36]

The general mechanisms for the electrochemical oxidation of glucose on Au electrodes have been reported in other literature studies.[31,34,36] The first step is the formation of $Au(OH)_{ads}$ (eq 1). The second step is the oxidation of glucose via the interaction between the hemiacetal group of glucose molecules,  , and $Au(OH)_{ads}$, which can be expressed as two processes: (1) the hydrogen bond to C_1 carbon in the hemiacetal group will be the first to be oxidized on the Au surface, forming radical species (eq 2). This process transfers one electron to the electrode. (2) These radical species are further oxidized to generate gluconolactone and transfer another electron to the electrode (eq 3). Finally, gluconolactone is desorbed from the electrode and hydrolyzed to form sodium gluconate in the PBS (eq 4). In other words, the generation of plentiful $Au(OH)_{ads}$ active sites (eq 1) and the rate of the dehydrogenation step (eqs 2 and 3) play important roles in the electro-oxidation of glucose on Au electrodes.

$$Au + H_2O \rightarrow AuOH^{(1-\lambda)-} + H^+ + \lambda e^- \quad (1)$$

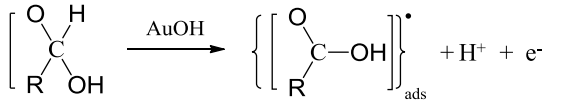

(2)

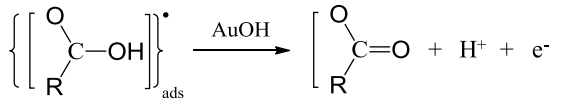

(3)

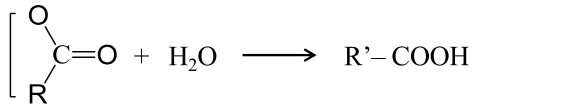

(4)

In our WSNFs, the Au nanowrinkles formed on two sides of the fiber as an electrocatalytic material did not completely cover the fiber, instead partially surrounded the outer surface of the rGO/PU fiber supporting matrix, which has many oxygen-containing functional groups. Therefore, the non-covalent interactions between the oxygen-containing groups on rGO and H_2O present near the active sites on the Au-coated area facilitate the formation of $Au(OH)_{abs}$ on the surface of the Au nanowrinkles,[37−39] which is critical for the dehydrogenation steps that initiate the glucose oxidation mechanism (eqs 2 and 3). Moreover, the oxygen-containing functional groups on the rGO flakes themselves also have noncovalent interactions with both the reactant (glucose) and the intermediate (adsorbed intermediate gluconolactone), which speeds dehydrogenation in the glucose oxidation mechanism.[37−39] Therefore, we expect that the synergetic effects between the rGO and Au nanowrinkles enhance the electrocatalytic effects for glucose oxidation.

To further scrutinize the electrocatalytic enhancement effects of the oxygen-containing functional groups in the rGO/PU fiber in the WSNFs, we fabricated WSNFs with various reduction times (30 min, 2, 4, 5, and 6 h) to vary the density of the oxygen-containing groups on rGO and then carried out electrochemical measurements. The CV curves in Figure 2c,d illustrate the glucose oxidation peaks of WSNF electrodes with various reduction times in 0.1 M PBS with 10 and 1 mM glucose, respectively. The oxidation peak current (I_{peak}) values as a function of reduction time, obtained from the data in Figure 2c,d, indicate that I_{peak} gradually increased as the reduction time decreased from 6 to 2 h and decreased as the reduction time was further decreased to 30 min (Figure 2e). We attribute these results to the change in the density of oxygen-containing functional groups on rGO in the fibers. When the reduction time is reduced, the increased number of oxygen-containing functional groups on rGO in the WSNF electrode might induce more $Au(OH)_{abs}$ and generate stronger noncovalent interactions with the intermediate and glucose species. As a result, WSNF electrodes with a short reduction time produced higher I_{peak} values than those with a longer reduction time. However, when the reduction time dropped to 30 min, more oxygen-containing functional groups remained on rGO, causing a drop in the I_{peak} and indicating a relatively less stable intermediate state exposed to very strong non-covalent interaction forces (such as hydrogen-bonding, electrostatic interaction forces, van der Waals forces, or

DOI: 10.1021/acsami.8b20583
ACS Appl. Mater. Interfaces 2019, 11, 10707−10717

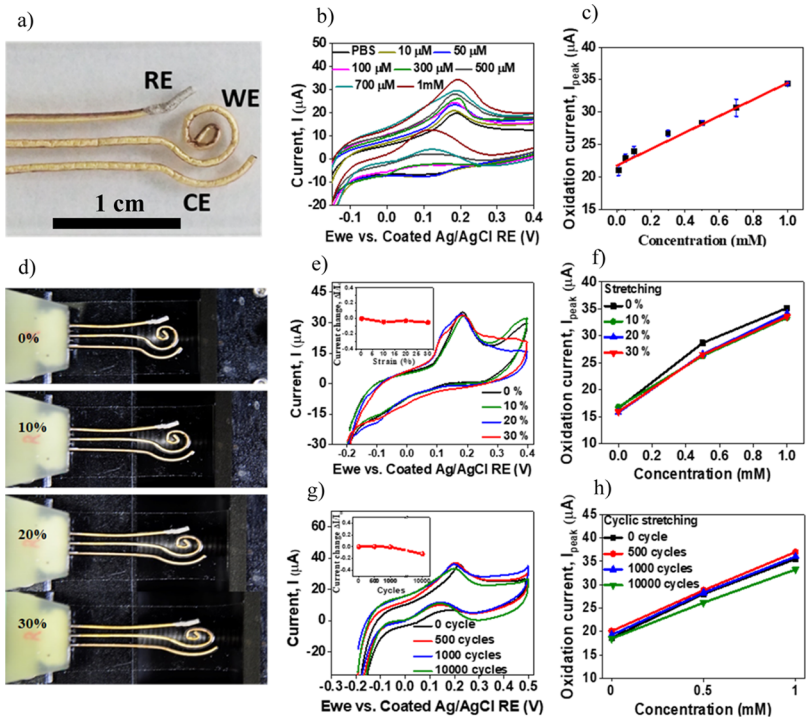

Figure 3. Characterization of the electrochemical WSNF glucose sensor. (a) Optical image of the WSNF glucose sensor. (b) CV plots of the fabricated device under various glucose concentrations. (c) I_{peak} of the WSNF glucose sensor as a linear function of glucose concentration. (d) Optical image of the WSNF glucose sensor on the PDMS substrate under stretching from 0 to 30%. (e) CV plots, (inset) current change, and (f) I_{peak} at various glucose concentrations of a WSNF glucose sensor under an applied strain of 0−30%. (g) CV plots, (inset) current change, and (h) I_{peak} at various glucose concentrations of a WSNF glucose sensor after cyclic stretching from 0 to 10 000 cycles.

hydrophobic interactions).[38] These results demonstrate that the optimum reduction time for WSNFs used as a WE for a highly sensitive nonenzymatic electrochemical glucose sensor is 2 h.

To further study the probable contribution of oxygen-containing functional groups in a glucose sensing mechanism, we fabricated two WSNF electrodes with a Au coating on one side and two sides of the fiber using the same reduction time. We expected these WSNF electrodes to have nearly the same number of oxygen-containing functional groups, but the number of them near the Au-coated area differed (the WSNF electrode coated with Au on two sides had more than that coated on only one side). The CV curves of the two WSNF electrodes in 0.1 M PBS with 10 mM glucose show that the I_{peak} of the WSNF electrode coated with Au on two sides was higher than that of the WSNF electrode coated with Au on one side by a factor of 3.4 (Figure 2f). In this experiment, the surface area of the Au nanowrinkles on the electrode coated on two sides was double that of the electrode coated on one side. In the ideal case, therefore, I_{peak} of the WSNF electrode coated on two sides should be two times higher than that of the WSNF electrode coated on one side, but the observed enhancement in I_{peak} was higher than that. Therefore, perhaps only the oxygen-containing functional groups on rGO near the Au-coated area enhance the electrocatalytic activity of the WSNF electrode.

To illustrate the formation of $Au(OH)_{abs}$, which is assisted by noncovalent interactions between the oxygen-containing functional groups on rGO and H_2O, we present a schematic (Figure 2g) for the formation of the $Au(OH)_{abs}$ layer on the WSNF electrodes made using various fabrication conditions: a WSNF with a short reduction time and a Au coating on two sides (Figure 2g(I)), a WSNF with a long reduction time fiber and a Au coating on two sides (Figure 2g(II)), and a WSNF with a short reduction time and a Au coating on one side (Figure 2g(III)). The fibers with a short reduction time and a Au coating on two sides present more oxygen-containing functional groups near the Au-coated area and more abundant formation of $Au(OH)_{abs}$ than the fibers with a long reduction time and a Au coating on two sides. For the fiber with a short time reduction and a Au coating on one side, only abundant oxygen-containing functional groups near the Au-coated area help to induce $Au(OH)_{abs}$.

To further investigate the role of oxygen-containing functional groups in enhancing the electrocatalytic activity of the WSNF electrode, we also measured the CVs of the WSNF, wrinkled PU/Au fiber with no rGO incorporated, and Au thin film electrodes with a similar geometric area in 0.1 M PBS with 10 mM glucose for comparison (Figure 2h). I_{peak} of the WSNF electrode was more than three times higher than that of the wrinkled PU/Au electrode with no rGO and more than 6.7 times higher than that of the Au thin film electrode. Those results again indicate that the oxygen-containing functional groups on rGO play an important role in glucose oxidation. We also carried out a CV scan of the WSNF electrode to it compared with that of an unwrinkled rGO/PU/Au fiber electrode in direct glucose oxidation. As depicted in Figure 2i, I_{peak} of the WSNF electrode is 1.4 times higher than that of the unwrinkled rGO/PU/Au fiber electrode. Therefore, the increase in the surface area caused by the Au nanowrinkles also contributes to the observed increase in electrocatalytic effects.

To study the sensitivity of the WSNF electrode to glucose, we measured the CV curves of the WSNF electrode with the

DOI: 10.1021/acsami.8b20583
ACS Appl. Mater. Interfaces 2019, 11, 10707−10717

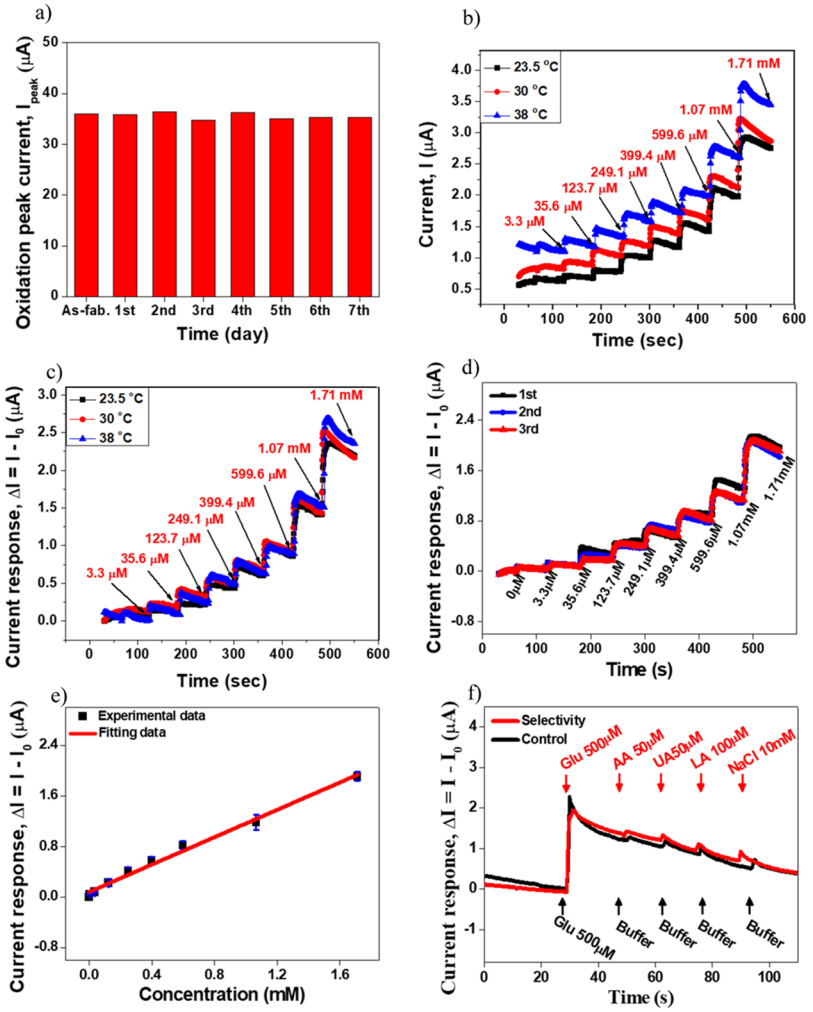

Figure 4. Performance of the electrochemical WSNF glucose sensor: stability, reliability, and selectivity. (a) I_{peak} of the as-fabricated WSNF glucose sensor in 1 mM glucose after 7 days of device storage in ambient conditions. (b) CA current signals of the WSNF glucose sensor at various glucose concentrations at temperatures of 23.5, 30, and 38 °C. (c) Replotted response current (ΔI) of the WSNF glucose sensor at various glucose concentrations at temperatures of 23.5, 30, and 38 °C. (d) Response currents (ΔI) of the WSNF glucose sensor at various glucose concentrations were measured three times. (e) Replotted response current (ΔI) of the WSNF glucose sensor as a linear function of glucose concentration. (f) Response current (ΔI) of the WSNF glucose sensor in 500 μM glucose with various interferents.

reduction time of 2 h under various glucose concentrations (Figure 2j). The WSNF electrode exhibited a broad detection range (0.5 nM to 10 mM) and high sensitivity. The I_{peak} value of the WSNF electrode to glucose is presented as an exponential function in low glucose concentration (Figure S5a) and as a linear function in medium and high glucose concentration ranges (Figure S5b,c, respectively). These results confirmed that the detection range of the WSNF electrode for glucose covers the range of glucose levels that occur in sweat.[9] Therefore, the WSNF holds promise as a WE for stretchable, electrochemical, nonenzymatic biosensors for continuous on-body monitoring of glucose in sweat.

To confirm that the WSNFs with a reduction time of 2 h can be used as electrodes in stretchable, electrochemical, non-enzymatic glucose sensors for continuous on-body monitoring of glucose in sweat, we evaluated the performance of a WSNF electrochemical sensor. We partially embedded free-standing WSNFs as the CE and WE and free-standing WSNF coated with Ag/AgCl on a PDMS substrate as the RE to fabricate a stretchable WSNF glucose sensor (Figure 3a), and then we tested the electrochemical performance of that fabricated device in its normal state and under mechanical deformation. Figure 3b shows the CV plots of the WSNF glucose sensor with glucose concentrations from 1 μM to 1 mM in PBS. The device with the Ag/AgCl-coated RE gave a negative shift of the glucose oxidation potential (Figure 3b) compared with that using a commercial Ag/AgCl/saturated KCl RE (Figure 2b). This phenomenon is contributed by probable difference in the components of Ag/AgCl ink in comparison with those of commercial Ag/AgCl/saturated KCl.

To confirm the reproducibility of the WSNF glucose sensor, we fabricated three devices and measured their CV curves in the same range of glucose concentration (1 μM to 1 mM). The results show that the I_{peak} values of the three devices were nearly the same (Figure S6). The average I_{peak} values extracted from the data in Figure S6 are presented as a linear function with glucose concentration in Figure 3c. Based on those results, we calculated a sensitivity of 140 $\mu A \cdot mM^{-1} \cdot cm^{-2}$. As shown by these results, the WSNF glucose sensor has high sensitivity to the glucose concentration in sweat from 1 μM to 1 mM. Therefore, it can be used for continuous on-body monitoring of glucose in sweat. Furthermore, the good

DOI: 10.1021/acsami.8b20583
ACS Appl. Mater. Interfaces 2019, 11, 10707−10717

electrocatalytic behavior of the WSNF glucose sensor is shown by the effect of the scan rate on CV performance (Figure S7a). The I_{peak} values linearly increase as the scan rate increases from 20 to 120 mV/s (Figure S7b). This indicates that a diffusion-controlled electrochemical process occurs on the WSNF electrode.

The durability of the stretchable WSNF glucose sensor under mechanical deformation is also an important parameter for reliable on-body measurement. To characterize the sensing performance under stretching, we applied a static strain from 0 to 30% to the sensor (Figure 3d) and measured the CV curves at various glucose concentrations. The CV plots (Figure 3e), current change (inset in Figure 3e), and I_{peak} values at various glucose concentrations (Figure 3f) demonstrate that the electrochemical performance of the device remained nearly unchanged under static mechanical deformation. We also tested the electrochemical performance of the stretchable WSNF glucose sensor under repetitive mechanical deformation using a cyclic stretching test. Figure 3g and its inset show the CV curves and oxidation current change, respectively, in a 1 mM glucose solution under cyclic stretching of 0, 500, 1000, and 10 000 cycles at a strain of 30%. The I_{peak} values at various glucose concentrations under cyclic stretching are presented in Figure 3h. These results indicate that the electrochemical performance of the device is stable under repetitive mechanical deformation, decreasing only slightly with cyclic stretching for up to 10 000 cycles. All those results confirm that the electrochemical WSNF glucose sensor has high sensitivity and excellent durability against mechanical deformation. For comparision with other wearable glucose sensors, selected wearable glucose sensors in the form factor of patch are presented in the Supporting Information Table S1.

To realize a stretchable, nonenzymatic glucose sensor based on WSNFs for continuous on-body monitoring of glucose in sweat, stability, reproducibility, and selectivity of the device should be also considered. We tested the stability of the WSNF glucose sensor by measuring its electrochemical performance in 1 mM glucose after storage in ambient conditions for 7 days. The results (Figure S8) indicate that the glucose oxidation potential of the device shifted in the negative direction as the storage time increased, but robust sensing performance was well maintained without a significant change in I_{peak} (Figure 4a). The negative shift of the oxidation potential might be caused by oxidization of the Ag/AgCl-coated RE during storage.

To evaluate its ability to monitor glucose in human sweat, the temperature dependence of the device performance should be also investigated because skin temperature changes during human activities. Figure 4b shows the chronoamperometric (CA) test results from the stretchable WSNF glucose sensor at an applied potential of 0.2 V with glucose concentrations from 0 to 1.71 mM in PBS at room temperature (23.5 °C), 30, and 38 °C. The baseline current of the CA curves showed a linearly increasing tendency as the temperature increased, possibly caused by the resistance change of the WSNF itself under temperature variation because of the thermal sensitivity of rGO.[40−42] However, the response current of the device, $\Delta I = I - I_o$, remained nearly unchanged at different temperatures (Figure 4c). Furthermore, to study the environmental temperature effect on the WSNF glucose sensor, the glucose sensor is attached to the human skin and the responsivity of the device to artificial sweat containing 200 μM glucose in summer with inside temperature (23.5 °C, room temperature with air conditioning) and outside temperature (32.5 °C). The results and detailed discussion are presented in Figure S9. Based on these results, we can conclude that the temperature does not contribute significantly to the glucose reaction, but the resistance of the fiber decreased as the temperature increased because of the presence of rGO.[40−42]

The reproducibility of the WSNF glucose sensor was studied using its amperometric response to glucose at various concentrations. Figure 4d presents ΔI of the sensor for three CA measurements; the sensor exhibited the same ΔI at each glucose concentration. Also, the extracted results present a linear relationship between ΔI and glucose concentration (Figure 4e), which can be used as a calibration curve for measuring the glucose concentration in sweat. Moreover, to demonstrate the repeatability of the sensor, we measured CA of the stretchable WSNF glucose sensor by injecting the glucose solutions four times with the same concentration at the saturation stage. The results and more detailed discussion are presented in Figure S10.

In sweat, several noteworthy interferents can affect sensor performance: uric acid (UA), ascorbic acid (AA), lactic acid (or derivatives of lactate) (LA), and sodium chloride (NaCl). Therefore, we examined the selectivity of the WSNF glucose sensor by verifying the effect of interferents in real-time measurements. We ran a CA plot with 0.2 V of applied voltage in 100 μL of PBS (0.1 M) for a baseline readout. We added 100 μL of 1 mM glucose solution to acquire a running baseline solution that was saturated at 500 μM glucose, and then we added 50 μL of each interferent solution, AA 50 μM, UA 50 μM, LA 100 μM, and NaCl 10 mM. For comparison, we added the same volume of PBS (instead of interferent solutions) as a control. The influence of the interferents is shown in the unchanged ΔI in a comparison of the selectivity (red) with the control line (black) in Figure 4f. All those results demonstrate that the WSNF glucose sensor has great selectivity against notable interferents in sweat and is suitable for a real sample demonstration. The high selectivity of the WSNF sensor can be attributed to the high roughness factor of the Au nanowrinkles. In glucose sensing, the electro-oxidation of glucose is controlled by a kinetic process, and thus it is very sensitive to the nanoscale crevices of Au nanowrinkles.[34,43] Meanwhile, the oxidation of the interferents (AA, UA, LA, and NaCl) is controlled by diffusion, which causes their surface concentration to be depleted immediately and completely under an applied anodic potential to the electrode. As a result, a reactant concentration gradient (a diffusion layer) is established near the surface of the Au nanowrinkles in the range of milliseconds, which depletes the interfering molecules from inside the crevices of the Au nanowrinkles.[34,43] Therefore, the oxidation of interferents does not significantly occur as long as glucose molecules can reach the crevice surface of the Au nanowrinkles.

Another great advantage of the glucose sensor based on WSNFs is that it can be directly integrated with stretchable fabric. A stretchable fabric that is lightweight, breathable, biocompatible, wearable, and has a high liquid absorption property is an ideal platform for continuous monitoring of glucose levels in sweat. The detailed processes by which the WSNF glucose sensor was fabricated onto the stretchable fabric are explained in the Methods and Figure S11. To observe the temperature changes of the human skin and both collect and store sweat samples, the WSNF glucose sensor was also integrated with a stretchable temperature sensor and

DOI: 10.1021/acsami.8b20583
ACS Appl. Mater. Interfaces 2019, 11, 10707−10717

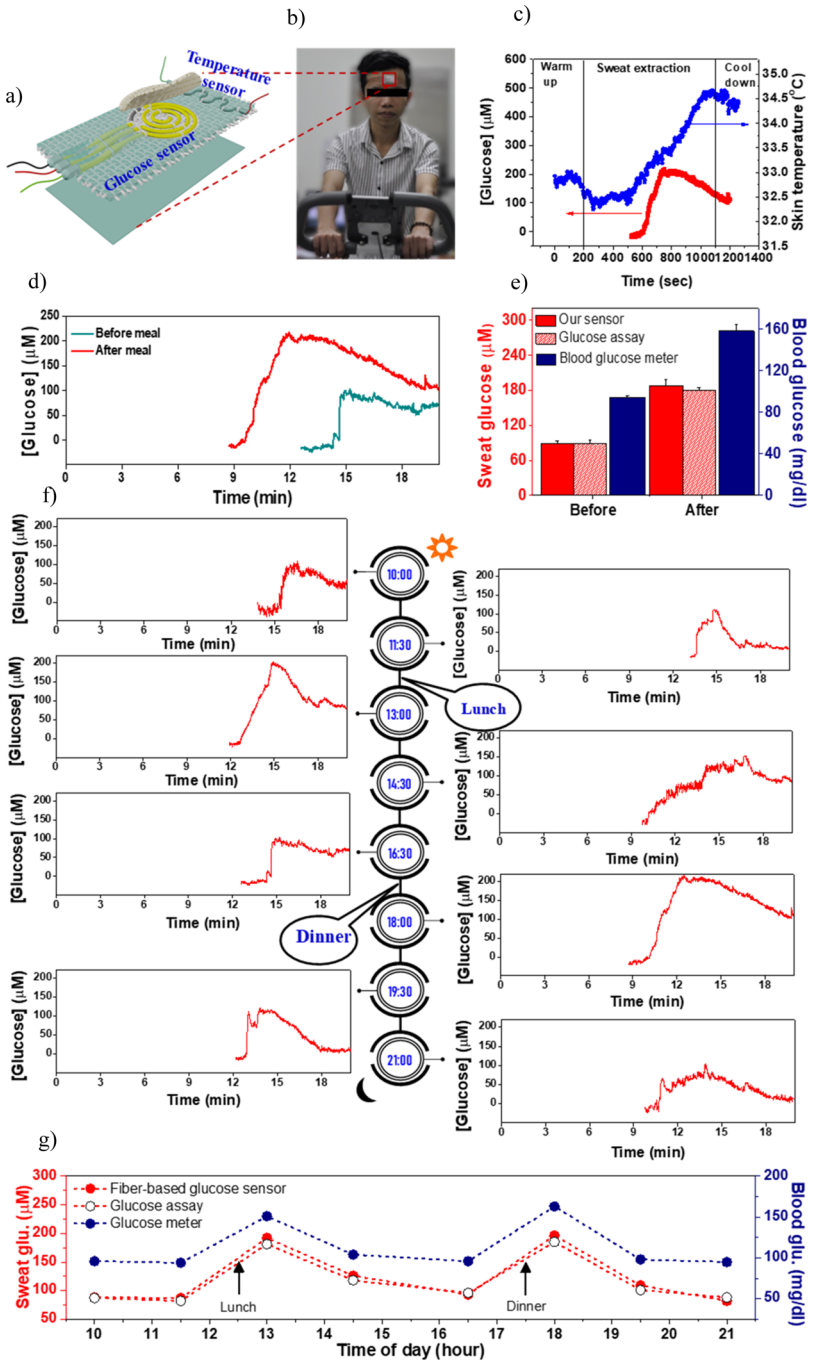

Figure 5. WSNF-based glucose sensor patch integrated with stretchable fabric for continuous on-body monitoring of glucose levels in human sweat. (a) Schematic diagram of the WSNF glucose sensor on stretchable fabric integrated with a stretchable temperature sensor. (b) The fabricated device was attached to the forehead of a subject for (c) continuous monitoring of skin temperature and the glucose levels in sweat. (d) Continuous on-body monitoring of glucose levels in sweat before and after meals. (e) Comparison of the glucose levels in sweat detected by the WSNF-based stretchable glucose sensor patch, a commercial sweat glucose assay, and the blood glucose level measured by a blood glucose meter. (f) Continuous on-body monitoring of glucose levels in sweat for 1 day. (g) Summary of the glucose levels measured in 1 day by the WSNF sweat glucose sensor, the commercial sweat glucose assay, and a blood glucose meter.

absorbent patch to generate a wearable glucose sensor patch (Figure 5a). The sensor patch was laminated onto the forehead of a human volunteer using an adhesive bandage (Figure 5b) and was electrically coupled to a portable electrochemical analyzer that can transfer the measured data to a smartphone via Bluetooth.

For continuous on-body monitoring of glucose in human sweat, two healthy subjects (males, 25 and 27 years old) with no medical history of diabetes participated in the study. To generate sweat, we used a cycling protocol. First, they cycled at a speed of 20 rpm to warm up for 3 min. Then, they cycled at 30 rpm for 14 min for the sweat extraction stage, and then they stopped cycling to cool the body down in 3 min. Figure 5c shows the continuous monitoring of skin temperature and glucose levels during cycling for the total time of 20 min. The temperature sensor monitored skin temperature changes, and

DOI: 10.1021/acsami.8b20583
ACS Appl. Mater. Interfaces 2019, 11, 10707−10717

we used those temperature data to correct the temperature-dependent glucose responsivity. Sweat was extracted after the first 3 min stage of cycling. At that time, the skin temperature was gradually cooling because of sweating, which is a natural mechanism of body temperature control, and the generated sweat was collected and stored by the absorption patch for glucose detection. While the perspiration continued, the sweat was stored until the sensor signal was saturated with enough sweat to enable glucose sensing and the skin temperature had become stable.

Figure 5d presents the results of continuous monitoring of glucose concentration before and after meals. The cycling protocol, as mentioned above, was used to generate the sweat before and after a meal. In case of the before-meal experiment, the perspiration seems to be very slow until 15 min after cycling. Here, the sweat is enough for glucose sensing until the signal is saturated and then slightly decreased. This is expectable because of the dilution effect on the increase of the sweating rate. The response is similar for the case of after-meal measurement. However, the perspiration starts earlier (10 min after cycling) and takes place massively in this case. The sweat glucose level after a meal was higher than before a meal. To confirm the accuracy and reliability of the patch, we measured the sweat glucose concentrations before and after meals three times and compared those results with measurements from a commercial sweat glucose assay kit and the blood glucose level as measured by a commercial blood glucose meter. The results in Figure 5e show that the sweat glucose concentrations measured by the sensor patch are well matched with those measured by the commercial assay kit. Furthermore, changes in the sweat glucose concentration are well correlated with the measured blood glucose concentrations (Figure 5e). To avoid an error or delay in sweat glucose concentration and blood glucose concentration, we collected sweat for analysis by the glucose assay kit while the participants were cycling for sweat generation, and we conducted the sweat glucose monitoring using the sensor patch immediately after extracting blood for measurement by the blood glucose meter. Data from 1 day of continuous on-body monitoring for sweat glucose are presented in Figure 5f. As summarized in the data, the sweat glucose levels measured by our patch matched well with the sweat glucose concentrations measured by the commercial assay kit and correlated well with the blood glucose concentration measured by the commercial blood glucose meter (Figure 5g).

CONCLUSIONS

In summary, we considered a unique approach to developing materials and designing and fabricating a new class of nonenzymatic glucose sensors based on free-standing WSNFs. As a WE, the WSNF demonstrated high sensitivity and low detection limit, which we attribute to the large surface area of the Au nanowrinkles and the high electrocatalytic activity facilitated synergistically by the oxygen-containing functional groups on the underlying rGO/PU fiber. The WSNF glucose sensor can be stretched up to 30% and offers high mechanical durability under repetitive cycles of mechanical deformation. In addition, the fabricated WSNF glucose sensor device presented high ambient-condition stability through the use of direct glucose oxidation without enzymes. The stretchable sensor also showed high selectivity against interferents and could be operated in neutral conditions because of the large surface area and nanoscale crevices of the Au nanowrinkles.

Taking advantage of its outstanding glucose sensing characteristics and simple fabrication, the WSNF glucose sensor can be directly sewn onto a stretchable fabric platform to create a glucose sensor patch and be attached to the human skin for continuous monitoring of glucose levels in sweat. The sweat glucose level measured by the sensor patch matches well with the level measured by a commercial sweat glucose assay kit and correlates well with blood glucose levels measured by a blood glucose meter. All our results indicate that the sensor patch based on WSNFs exhibits high performance in continuous sweat glucose detection. Therefore, WSNFs hold promise for use as stretchable, nonenzymatic, wearable, self-testing, electrochemical glucose sensors. Future work will focus on integrating the stretchable glucose sensor with a microfluidic biofluid handling device that will collect and store the sweat sample to prevent a dilution effect and improve the accuracy of continuous monitoring.

METHODS

Fabrication of the rGO/PU Nanocomposite Fiber. The rGO/PU nanocomposite fibers were produced by a wet spinning method. Briefly, the liquid phase blending method was used to prepare the rGO/PU solution. PU (SG 85 A from Teco Flex) was dissolved in dimethylacetamide (DMAC, Sigma-Aldrich) with a concentration of 0.3 g/mL. Graphene oxide nanosheets (GO, prepared by the modified Hummers method) dispersed in DMAC at a concentration of 5 mg/mL were mixed with appropriate weight fractions of PU solution and stirred for 12 h. The rGO/PU solution was injected into a water bath and kept there for 5 min to form PU/GO-gel fibers. They were reduced in 1 wt % solution of AA (Sigma-Aldrich) in deionized water (DI water) for the desired reduction time in an oven at 100 °C. Then, they were taken out, rinsed, and immersed in DI water overnight at room temperature. Finally, the PU/rGO-gel fibers were dried in an oven at 120 °C for 2 h to form PU/rGO nanocomposite fibers.

Fabrication of WSNFs from the rGO/PU/Au Nanohybrid. The rGO/PU nanocomposite fiber was prestretched up to 100% on a high-temperature plastic holder. The stretched fibers were treated with an oxygen microwave plasma for 30 s. A 5 nm-thick Cr layer and 60 nm-thick Au layer were deposited by e-beam and thermal evaporation, respectively, on one side of the stretched fiber and then on the other side after rotating 180°. The Au-deposited rGO/PU fibers were then taken from the holder. The wrinkled surface formed after releasing the deposited fibers.

Fabrication of the Electrochemical WSNF Glucose Sensor. To make the WSNF glucose sensor on a PDMS substrate, we coated a completely cured PDMS (10:1, w/w ratio of base to curing agent) substrate with a liquid PDMS (10:1) layer to a thickness of 0.5 mm by spin-coating at 2500 rpm, for a total thickness of around 30 μm. Then, the substrate was partially cured in an oven at 80 °C for 3 min to form a sticky surface. The formed fiber electrodes were put on the sticky PDMS substrate and then completely cured in an oven at 80 °C for 30 min. The electrode area was surrounded by a PDMS well to contain the analyte solution for characterization.

Integration of the Electrochemical WSNF Glucose Sensor with Stretchable Fabric. To prepare the textile-based substrate, we bought a stretchable cotton fabric and nylon thread at a local fabric market (Seoul, Republic of Korea). To make the opening fabric region, we placed the washed fabric on a plate surface. Gelatin (Sigma-Aldrich) of 10 wt % in DI water was boiled at 100 °C for 5 min. Then, 50 μL of gelatin was dropped onto the fabric to form a circular region with a diameter of 1 cm. We put the fabric into the refrigerator for 15 min to solidify the gelatin. PDMS (10:1) was coated on the substrate using a spin coating machine at 1000 rpm and then cured in an oven at 80 °C for 1 h.

DOI: 10.1021/acsami.8b20583
ACS Appl. Mater. Interfaces 2019, 11, 10707−10717

The substrate was rubbed with a brush and then sonicated with 0.1 M NaOH for 20 min to remove the gelatin and mercerize the opening in the fabric. We then washed the fabric using DI water and dried it at 60 °C under an air supply for 1 h.

We used a sewing needle and the stretchable nylon thread to sew the WSNF electrodes directly onto the fabric substrate. The circular fabric absorbent pad, which was also sewn to the substrate, has the same diameter as the opening in the fabric. A thin sticky PDMS layer was prepared to cover the back side of the opening in the fabric.

We connected three copper wires to the three electrodes using a Ag-epoxy paste (1:1) (Epoxy Technology Inc.) and then cured it in an oven at 80 °C for 2 h. In the end, the thin PDMS encapsulation covered the whole substrate around the electrode.

Measurements of Sweat Glucose Concentration on a Human Forehead. The forehead skin of each subject was cleaned using medical alcohol bought at a local pharmacy (Suwon, Republic of Korea). The patch glucose sensor was attached to the forehead of each volunteer by an adhesive bandage and connected to a portable potentiostat (PStouch-PalmSens) that was wirelessly controlled by an app on a smartphone. The CV data were acquired at an applied voltage of 0.2 V. To confirm the accuracy and reliability of the glucose patch, the sweat glucose concentration was also measured using a commercial glucose assay kit (no. 10009582, Cayman chemical), and to observe the correlation between sweat glucose and blood glucose levels, we used a glucometer (i-Sens, CareSens N) to measure the glucose concentration in finger-pricked blood from the same subjects. The human subjects research was carried out after the approval of the Institutional Review Board (IRB) at the University, and all glucose measurements from the two subjects (male, age: 25 and 27) were conducted after receiving informed signed consent from them.

■ ASSOCIATED CONTENT

Supporting Information

The Supporting Information is available free of charge on the ACS Publications website at DOI: 10.1021/acsami.8b20583.

Optical images of the wet spinning system and fabrication process for the rGO/PU nanocomposite fiber; schematic diagram of the fabrication process for WSNFs of rGO/PU/Au; $I-V$ curves and resistance change of WSNF under applied strain from 0 to 70%; schematic diagram presenting the fabrication of the electrochemical glucose sensor using WSNFs as the WE and a commercial Ag/AgCl/saturated KCl and Pt wire as the RE and CE, respectively; I_{peak} of the WSNF electrode in various glucose concentration; CV curves and I_{peak} values of three WSNF glucose sensors with the same fabrication conditions; CV curves and I_{peak} values of the WSNF glucose sensor at various scan rates; CV curves of the WSNF glucose sensor in 1 mM glucose solution after storage at ambient conditions for 7 days; CA current signals of the WSNF glucose sensor response to artificial sweat with 200 μM glucose concentration at outside and inside temperature; CA response of the stretchable WSNF glucose sensor by injecting the glucose solutions with the same concentration four times at the saturation stage; schematic diagram presenting the fabrication process of the WSNF glucose sensor on stretchable fabric; and table presenting the selected wearable glucose sensor in form factor of patch (PDF)

■ AUTHOR INFORMATION

Corresponding Author

*E-mail: nelee@skku.edu.

ORCID

Nae-Eung Lee: 0000-0002-6539-5010

Author Contributions

P.T.T. and T.Q.T. contributed equally to this work. T.Q.T. designed the concept. T.Q.T. and P.T.T. carried out the experiments. T.M.L.D. contributed to the fabrication of the rGO/PU fibers. C.W.B. contributed to CV measurement. T.Q.T. and P.T.T. contributed to data analysis and manuscript preparation. T.Q.T. and N.-E.L. wrote the paper, and N.-E.L. supervised the project.

Notes

The authors declare no competing financial interest.

■ ACKNOWLEDGMENTS

This research was supported by the Basic Science Research Program (2016R1A2A1A05005423) and the Korean Research Fellowship Program (2015H1D3A1062350) through the National Research Foundation (NRF) funded by the Ministry of Science, ITC, and Future Planning.

■ REFERENCES

(1) Wang, J. Electrochemical Glucose Biosensors. *Chem. Rev.* **2008**, *108*, 814−825.

(2) Senior, M. Novartis Signs Up for Google Smart Lens. *Nat. Biotechnol.* **2014**, *32*, 856.

(3) Yao, H.; Shum, A. J.; Cowan, M.; Lähdesmäki, I.; Parviz, B. A. A Contact Lens with Embedded Sensor for Monitoring Tear Glucose Level. *Biosens. Bioelectron.* **2011**, *26*, 3290−3296.

(4) Tierney, M. J.; Tamada, J. A.; Potts, R. O.; Jovanovic, L.; Garg, S. Clinical evaluation of the GlucoWatch biographer: a continual, non-invasive glucose monitor for patients with diabetes. *Biosens. Bioelectron.* **2001**, *16*, 621−629.

(5) Bandodkar, A. J.; Jia, W.; Yardımcı, C.; Wang, X.; Ramirez, J.; Wang, J. Tattoo-Based Noninvasive Glucose Monitoring: A Proof-of-Concept Study. *Anal. Chem.* **2015**, *87*, 394−398.

(6) Lee, H.; Choi, T. K.; Lee, Y. B.; Cho, H. R.; Ghaffari, R.; Wang, L.; Choi, H. J.; Chung, T. D.; Lu, N.; Hyeon, T.; Choi, S. H.; Kim, D.-H. A Graphene-Based Electrochemical Device with Thermoresponsive Microneedles for Diabetes Monitoring and Therapy. *Nat. Nanotechnol.* **2016**, *11*, 566−572.

(7) Koh, A.; Kang, D.; Xue, Y.; Lee, S.; Pielak, R. M.; Kim, J.; Hwang, T.; Min, S.; Banks, A.; Bastien, P.; Manco, M. C.; Wang, L.; Ammann, K. R.; Jang, K.-I.; Won, P.; Han, S.; Ghaffari, R.; Paik, U.; Slepian, M. J.; Balooch, G.; Huang, Y.; Rogers, J. A. A Soft, Wearable Microfluidic Device for The Capture, Storage, and Colorimetric Sensing of Sweat. *Sci. Transl. Med.* **2016**, *8*, 366ra165.

(8) Chen, Y.; Lu, S.; Zhang, S.; Li, Y.; Qu, Z.; Chen, Y.; Lu, B.; Wang, X.; Feng, X. Skin-Like Biosensor System via Electrochemical Channels for Noninvasive Blood Glucose Monitoring. *Sci. Adv.* **2017**, *3*, No. e1701629.

(9) Lee, H.; Song, C.; Hong, Y. S.; Kim, M. S.; Cho, H. R.; Kang, T.; Shin, K.; Choi, S. H.; Hyeon, T.; Kim, D.-H. Wearable/Disposable Sweat-Based Glucose Monitoring Device with Multistage Transdermal Drug Delivery Module. *Sci. Adv.* **2017**, *3*, No. e1601314.

(10) Martín, A.; Kim, J.; Kurniawan, J. F.; Sempionatto, J. R.; Moreto, J. R.; Tang, G.; Campbell, A. S.; Shin, A.; Lee, M. Y.; Liu, X.; Wang, J. Epidermal Microfluidic Electrochemical Detection System: Enhanced Sweat Sampling and Metabolite Detection. *ACS Sens.* **2017**, *2*, 1860−1868.

(11) Gao, W.; Emaminejad, S.; Nyein, H. Y. Y.; Challa, S.; Chen, K.; Peck, A.; Fahad, H. M.; Ota, H.; Shiraki, H.; Kiriya, D.; Lien, D.-H.; Brooks, G. A.; Davis, R. W.; Javey, A. Fully Integrated Wearable Sensor Arrays for Multiplexed In Situ Perspiration Analysis. *Nature* **2016**, *529*, 509−514.

(12) Zhang, Z.; Liu, H.; Deng, J. A Glucose Biosensor Based on Immobilization of Glucose Oxidase in Electropolymerizedo-Amino-

DOI: 10.1021/acsami.8b20583
ACS Appl. Mater. Interfaces 2019, 11, 10707−10717

phenol Film on Platinized Glassy Carbon Electrode. *Anal. Chem.* **1996**, *68*, 1632−1638.
(13) Wu, B.; Zhang, G.; Shuang, S.; Choi, M. M. F. Biosensors for Determination of Glucose with Glucose Oxidase Immobilized on An Eggshell Membrane. *Talanta* **2004**, *64*, 546−553.
(14) Wilson, R.; Turner, A. P. F. Glucose Oxidase: An Ideal Enzyme. *Biosens. Bioelectron.* **1992**, *7*, 165−185.
(15) Zhu, H.; Li, L.; Zhou, W.; Shao, Z.; Chen, X. Advances in Non-Enzymatic Glucose Sensors Based on Metal Oxides. *J. Mater. Chem. B* **2016**, *4*, 7333−7349.
(16) Dong, X.-C.; Xu, H.; Wang, X.-W.; Huang, Y.-X.; Chan-Park, M. B.; Zhang, H.; Wang, L.-H.; Huang, W.; Chen, P. 3D Graphene-Cobalt Oxide Electrode for High-Performance Supercapacitor and Enzymeless Glucose Detection. *ACS Nano* **2012**, *6*, 3206−3213.
(17) Lang, X.-Y.; Fu, H.-Y.; Hou, C.; Han, G.-F.; Yang, P.; Liu, Y.-B.; Jiang, Q. Nanoporous Gold Supported Cobalt Oxide Microelectrodes as High-Performance Electrochemical Biosensors. *Nat. Commun.* **2013**, *4*, 2169.
(18) Cheng, X.; Zhang, J.; Chang, H.; Luo, L.; Nie, F.; Feng, X. High Performance Cu/Cu2O Nanohybrid Electrocatalyst for Nonenzymatic Glucose Detection. *J. Mater. Chem. B* **2016**, *4*, 4652−4656.
(19) Marioli, J. M.; Kuwana, T. Electrochemical Detection of Carbohydrates at Nickel-Copper and Nickel-Chromium-Iron Alloy Electrodes. *Electroanalysis* **1993**, *5*, 11−15.
(20) Marioli, J. M.; Luo, P. F.; Kuwana, T. Nickel-chromium alloy electrode as a carbohydrate detector for liquid chromatography. *Anal. Chim. Acta* **1993**, *282*, 571−580.
(21) Zhai, D.; Liu, B.; Shi, Y.; Pan, L.; Wang, Y.; Li, W.; Zhang, R.; Yu, G. Highly Sensitive Glucose Sensor Based on Pt Nanoparticle/Polyaniline Hydrogel Heterostructures. *ACS Nano* **2013**, *7*, 3540−3546.
(22) Chen, K.-J.; Su, W.-N.; Pan, C.-J.; Cheng, S.-Y.; Rick, J.; Wang, S.-H.; Liu, C.-C.; Chang, C.-C.; Yang, Y.-W.; Wang, C.-H.; Hwang, B.-J. Dendritic Platinum-Decorated Gold Nanoparticles for Non-Enzymatic Glucose Biosensing. *J. Mater. Chem. B* **2013**, *1*, 5925−5932.
(23) Zhang, A.; Tian, Y.; Liu, M.; Xiao, Y.; Jia, D.; Li, F. Enhanced Performances of Nonenzymatic Glucose Sensors by Attaching Au Nanoparticles onto The Surfaces of Cu2O@Cu Nanocable Arrays. *RSC Adv.* **2014**, *4*, 43973−43976.
(24) Niu, X.; Lan, M.; Zhao, H.; Chen, C. Highly Sensitive and Selective Nonenzymatic Detection of Glucose Using Three-Dimensional Porous Nickel Nanostructures. *Anal. Chem.* **2013**, *85*, 3561−3569.
(25) Madhu, R.; Veeramani, V.; Chen, S.-M.; Manikandan, A.; Lo, A.-Y.; Chueh, Y.-L. Honeycomb-like Porous Carbon-Cobalt Oxide Nanocomposite for High-Performance Enzymeless Glucose Sensor and Supercapacitor Applications. *ACS Appl. Mater. Interfaces* **2015**, *7*, 15812−15820.
(26) Fu, S.; Fan, G.; Yang, L.; Li, F. Non-Enzymatic Glucose Sensor Based on Au Nanoparticles Decorated Ternary Ni-Al Layered Double Hydroxide/Single-Walled Carbon Nanotubes/Graphene Nanocomposite. *Electrochim. Acta* **2015**, *152*, 146−154.
(27) Wu, K.-L.; Cai, Y.-M.; Jiang, B.-B.; Cheong, W.-C.; Wei, X.-W.; Wang, W.; Yu, N. Cu@Ni core-shell nanoparticles/reduced graphene oxide nanocomposites for nonenzymatic glucose sensor. *RSC Adv.* **2017**, *7*, 21128−21135.
(28) Ramachandran, K.; Raj kumar, T.; Babu, K. J.; Gnana kumar, G. Ni-Co Bimetal Nanowires Filled Multiwalled Carbon Nanotubes for The Highly Sensitive and Selective Non-Enzymatic Glucose Sensor Applications. *Sci. Rep.* **2016**, *6*, 36583.
(29) Oh, S. Y.; Hong, S. Y.; Jeong, Y. R.; Yun, J.; Park, H.; Jin, S. W.; Lee, G.; Oh, J. H.; Lee, H.; Lee, S.-S.; Ha, J. S. Skin-Attachable, Stretchable Electrochemical Sweat Sensor for Glucose and pH Detection. *ACS Appl. Mater. Interfaces* **2018**, *10*, 13729−13740.
(30) Moyer, J.; Wilson, D.; Finkelshtein, I.; Wong, B.; Potts, R. Correlation Between Sweat Glucose and Blood Glucose in Subjects with Diabetes. *Diabetes Technol. Ther.* **2012**, *14*, 398−402.
(31) Prehn, R.; Cortina-Puig, M.; Muñoz, F. X. A Non-Enzymatic Glucose Sensor Based on the Use of Gold Micropillar Array Electrodes. *J. Electrochem. Soc.* **2012**, *159*, F134−F139.
(32) Niu, X.; Li, X.; Pan, J.; He, Y.; Qiu, F.; Yan, Y. Recent Advances in Non-Enzymatic Electrochemical Glucose Sensors Based on Non-Precious Transition Metal Materials: Opportunities and Challenges. *RSC Adv.* **2016**, *6*, 84893−84905.
(33) Hsu, C.-W.; Su, F.-C.; Peng, P.-Y.; Young, H.-T.; Liao, S.; Wang, G.-J. Highly Sensitive Non-Enzymatic Electrochemical Glucose Biosensor Using A Photolithography Fabricated Micro/Nano Hybrid Structured Electrode. *Sens. Actuators, B* **2016**, *230*, 559−565.
(34) Chen, L. Y.; Lang, X. Y.; Fujita, T.; Chen, M. W. Nanoporous Gold for Enzyme-Free Electrochemical Glucose Sensors. *Scr. Mater.* **2011**, *65*, 17−20.
(35) Adams-McGavin, R. C.; Chan, Y.; Gabardo, C. M.; Yang, J.; Skreta, M.; Fung, B. C.; Soleymani, L. Nanoporous And Wrinkled Electrodes Enhance The Sensitivity of Glucose Biosensors. *Electrochim. Acta* **2017**, *242*, 1−9.
(36) Hsiao, M. W.; Adžić, R. R.; Yeager, E. B. Electrochemical Oxidation of Glucose on Single Crystal and Polycrystalline Gold Surfaces in Phosphate Buffer. *J. Electrochem. Soc.* **1996**, *143*, 759−767.
(37) Ismail, N. S.; Le, Q. H.; Yoshikawa, H.; Saito, M.; Tamiya, E. Development of Non-enzymatic Electrochemical Glucose Sensor Based on Graphene Oxide Nanoribbon - Gold Nanoparticle Hybrid. *Electrochim. Acta* **2014**, *146*, 98−105.
(38) Hoa, L. Q.; Vestergaard, M. d. C.; Yoshikawa, H.; Saito, M.; Tamiya, E. Enhancing Catalytic Performance of Pt-Based Electrodes With A Noncovalent Interaction-Induced Functionalized Carbon Nanotube-Grafted Matrix. *J. Mater. Chem.* **2012**, *22*, 14705−14714.
(39) Hoa, L. Q.; Vestergaard, M. d. C.; Yoshikawa, H.; Saito, M.; Tamiya, E. Functionalized Multi-Walled Carbon Nanotubes as Supporting Matrix For enhanced Ethanol Oxidation on Pt-Based Catalysts. *Electrochem. Commun.* **2011**, *13*, 746−749.
(40) Trung, T. Q.; Tien, N. T.; Kim, D.; Jung, J. H.; Yoon, O. J.; Lee, N.-E. High Thermal Responsiveness of A Reduced Graphene Oxide Field-Effect Transistor. *Adv. Mater.* **2012**, *24*, 5254−5260.
(41) Trung, T. Q.; Ramasundaram, S.; Hong, S. W.; Lee, N.-E. Flexible and Transparent Nanocomposite of Reduced Graphene Oxide and P(VDF-TrFE) Copolymer for High Thermal Responsivity in a Field-Effect Transistor. *Adv. Funct. Mater.* **2014**, *24*, 3438−3445.
(42) Trung, T. Q.; Le, H. S.; Dang, T. M. L.; Ju, S.; Park, S. Y.; Lee, N.-E. Freestanding, Fiber-Based, Wearable Temperature Sensor with Tunable Thermal Index for Healthcare Monitoring. *Adv. Healthcare Mater.* **2018**, *7*, 1800074.
(43) Yuan, J. H.; Wang, K.; Xia, X. H. Highly Ordered Platinum-Nanotubule Arrays for Amperometric Glucose Sensing. *Adv. Funct. Mater.* **2005**, *15*, 803−809.

DOI: 10.1021/acsami.8b20583
ACS Appl. Mater. Interfaces 2019, 11, 10707−10717